

**Chandra X-ray Observations of RX J1053.7+5735: A High-Redshift
Early-Stage Cluster Merger**

Ben Cohen
Research under Professor Craig Sarazin

Submitted May 2024
Department of Astronomy at the University of Virginia

This thesis is submitted in partial completion of the requirements of the
BS Astronomy-Physics Major

Intended Graduation Date of May 2025

Chandra X-ray Observations of RX J1053.7+5735: A High-Redshift Early-Stage Cluster Merger

Ben Cohen¹, Alex Rosenthal¹, Vibha Velmurugan¹, Zaina Tarafder¹, Efrain Perez¹,
and Craig L. Sarazin¹*

¹*Department of Astronomy, University of Virginia, P.O. Box 400325, Charlottesville, VA 22904, USA*

Accepted XXX. Received YYY; in original form ZZZ

ABSTRACT

Nine observations were taken of RX J1053.7+5735. The FAINT mode observation 4936 from 2004 was evaluated against the eight VFAINT mode observations from 2021–2022, with the result of keeping it with the rest of the analysis. Multiple broad band images were created, including a merged exposure map and an adaptively-smoothed image focusing on the desired cluster. The system is clearly bimodal, and undergoing a merger. Further images were produced to observe the soft, medium, and hard X-rays. The cores of the two subclusters have softer X-ray emission, indicating they are cooler. This may indicate that the cluster cool cores remain at least partially intact. There is an extension of the system to the NNE; it appears to be softer (cooler) than the bulk of the cluster. However, no clear evidence of a merger shock was found.

Key words: galaxies: clusters: general — galaxies: clusters: individual (RX J1053.7+5735) — galaxies: clusters: intracluster medium — galaxies: elliptical and lenticular, cD — radio continuum: general — X-rays: galaxies: clusters

1 INTRODUCTION

Clusters of galaxies form by the merger of smaller galaxian systems. These mergers are the most energetic events since the Big Bang, involving total energies of 10^{64} ergs. Merger shocks driven into the intracluster gas are the primary heating mechanism in massive clusters. *Chandra* and *XMM* have provided beautiful X-ray images and spectra of merger hydrodynamical effects, including “cold fronts” and merger shocks (e.g., Markevitch & Vikhlinin 2007). Although most of the cluster mergers which have been studied are at relatively low redshifts, mergers are expected to have occurred over a significant fraction of the lifespan of the Universe, from $z \sim 2$ to the present.

Clusters of galaxies have long been vital probes of cosmology, giving early evidence of dark matter and of a low density Universe. Their importance is partly due to their being simultaneously the biggest objects which are relaxed and bound, and the smallest objects which contain a fair sample of the composition of the Universe (e.g. baryons vs. dark matter). However, the use of clusters for cosmology generally requires that their total masses be determined. This is often done using mass proxies from X-ray or Sunyaev-Zel’dovich (SZ) data, which depend on clusters being relaxed. For example, the integrated SZ signal (Compton Y) measures the total thermal content of the electrons in the intracluster medium (ICM), which is equivalent to the integrated pressure and should be

closely connected to the mass if the gas is in hydrostatic equilibrium. For the study of high redshift clusters to constrain cosmology, observations of the SZ effect are particularly useful, since they are relatively independent of redshift and distance.

Unfortunately, cluster mergers can effect X-ray and SZ mass determinations. Mergers produce significant boosts in cluster X-ray luminosities and temperatures (Randall, Sarazin, & Ricker 2002). They also produce localized increases in the SZ Y, and an oscillatory increase and decrease in the integrated SZ Y (Wik, Sarazin et al. 2008). These merger effects can be assessed with high spatial resolution X-ray (i.e., *Chandra*) and SZ observations.

RX J1053.7+5735 (hereafter RXJ1053) is a high redshift ($z = 1.134$; Hashimoto et al. 2005 [Hash5]) cluster, which was first discovered in very deep ROSAT HRI observations of the Lockman Hole region (Hasinger et al. 1998a). The total X-ray flux is 2×10^{14} erg cm²s⁻¹ (0.5–2 keV). One bright galaxy projected within the east subcluster had a spectroscopic redshift of 1.26; Hashimoto et al. (2004 [Hash4]) concluded that this galaxy was probably a background object. There is another bright galaxy in the east subcluster which is probably the Brightest Cluster Galaxy (BCG) for this subcluster.

A deep *XMM* observation of the Lockman Hole provided more detailed information on the cluster (Hashimoto et al. 2002, 2004). The total cluster spectrum gave a temperature of 3.9 ± 0.2 keV, an iron abundance of $0.46^{+0.11}_{-0.07}$ solar, and an X-ray redshift of $z = 1.14 \pm 0.01$. This cluster redshift was confirmed by optical/IR spectra of six galaxies (Hash5). The unabsorbed flux is 2.8×10^{-14} erg

* E-mail: sarazin@virginia.edu

$\text{cm}^{-2}\text{s}^{-1}$ (0.2–10 keV), giving a luminosity of 2.4×10^{44} erg s^{-1} (0.2–10 keV).

The west subcluster was found to be hotter and more luminous than the east subcluster. The X-ray hardness ratio map also suggested that the region between the two subclusters is hotter than either cluster. This would be consistent with an early-stage merger with a shocked region between the two clusters, as expected from numerical simulations of clusters and observations of nearby, early-stage cluster mergers (e.g., Cyg-A; Sarazin et al. 2013). Hash4 suggested that there is a cold front between the west subcluster and the shock region between the clusters, and that the west subcluster has a central cool core.

In §2 we describe the *Chandra* observations and basic data reduction processes.

2 CHANDRA OBSERVATIONS AND DATA ANALYSIS

RXJ1053 was observed nine times with the *Chandra* X-ray Observatory (Table 1). In all of the observations, the ACIS-S detector was used, with the cluster on the S3 chip (chip 7). The first observation was done in 2004 (OBSID 4936, PI Peter Predehl); this first observation was done in FAINT mode. We added a series of eight observations in 2021–2022 (PI Craig Sarazin). The last eight observations were done with the ACIS-S detector in VFaint mode.

The data analysis was done primarily using HEASARC version 6.26.1¹ and CIAO version 4.14². X-ray spectra were fit using XSPEC version 12.10.1f³. Each of the observations was reprocessed using the CIAO command `CHANDRA_REPRO` to insure that the calibrations were up-to-date. We utilized the extra information available in VFaint mode to reject additional particle background events in the last eight observations. We checked each observation for background flares using the CIAO `DEFLARE` routine. The first observations (OBSID 4936) had a large background flare that biased the mean flux significantly. We removed this flare from the observation Good Time Intervals (GTIs) by hand before running `DEFLARE`. The initial exposures and cleaned exposures are shown in Table 1 for each of the observations.

The CIAO `WAVDETECT` algorithm was used to detect point sources in each observation using images in the 0.5–7.0 keV band. The point-spread-function was determined as a function of position on the S3 chip for each observation using the CIAO routine `MKPSFMAP`. The detection significance threshold was set at 10^{-6} , and wavelet scales of 1, 2, 4, 16, and 32 pixels were used. The resulting sources were examined, and any false or likely extended sources were removed. The positions of the point sources in the different observations agreed, so no further alignment of the images was needed.

Figure 1 displays the resulting broad band exposure map from merging the nine observations. The observations were taken at a wide range of roll angles. However, the exposure is fairly uniform in the central region where the cluster is located.

Blank sky background images for broad, hard, medium, and soft bands were created for the individual observation images, and the CIAO routine `DMIMGCALC` was used to create broad, hard, medium, and soft background images for the nine merged observations. A similar process was used in merging only the eight observations that were done in VFaint mode as a means of comparison.

Table 1. *Chandra* observations.

OBSID	Date	Mode ^a	Exposure (ksec)	Clean Exposure (ksec)
4936	2004-07-24	F	92.24	72.79
23842	2021-11-15	VF	38.60	36.30
24394	2021-11-10	VF	30.21	30.21
24395	2021-11-13	VF	26.76	25.08
24396	2022-01-13	VF	29.72	28.18
24397	2022-01-23	VF	27.06	26.03
24398	2021-11-11	VF	28.24	28.24
24399	2022-02-06	VF	19.85	18.83
24400	2021-11-20	VF	20.84	20.84
Total			313.52	286.50

Table Note: ^a F = Faint, VF = Very Faint

□

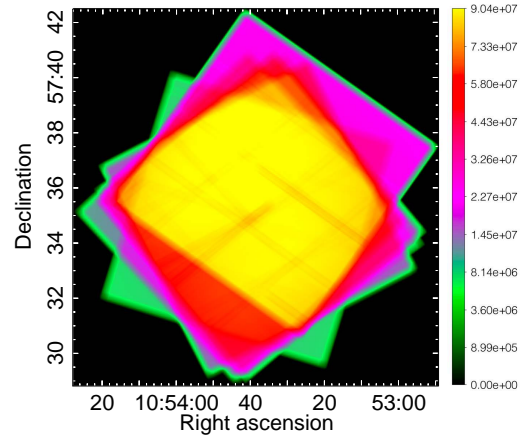


Figure 1. Broad band exposure map of the merged nine observations. Linear colorbar units in $\text{cm}^2 \text{s}$.

Excluding the observation done in FAINT mode did not significantly impact the data analyzed, so the nine merged observations were used from this point onward.

In Figure 1, it can be seen that the right ascension ranges from approximately 10:52:50 to 10:54:28 and that the declination ranges from approximately 57:31 to 57:42.5. To obtain images focused on the cluster of interest, the cluster’s extent had to be determined, which required creating an exposure and background corrected image. Using `FARITH`, the background was subtracted, and then the result was divided by the exposure. Within DS9, a color of `b`, a scaling of square root, and a minimum scale parameters value of 0 were applied to this image. A rectangle region was selected for all of the remaining images of the cluster. The corners of the rectangle were used to determine `XMIN` = 3938, `XMAX` = 4321, `YMIN` = 4075, and `YMAX` = 4332 (these numbers refer to the physical coordinates in the display). A new image was created by copying this image and binning it using `XMIN`, `XMAX`, `YMIN`, and `YMAX`. The resulting image is shown in Figure 2, which has right ascension ranging from approximately 10:53:31 to 10:53:55 and declination ranging from approximately 57:34:45 to 57:36:30. This image includes scale: `sqrt`, color: `a`, scale parameters with `zmin` = $1.35\text{e-}09$ and `zmax` = $1\text{e-}08$, and smooth parameters with `radius` = 2 and `sigma` = 1.

The perl script `ASMOOTH` was used for creating an adaptively-smoothed broad band image. Prior to this, all point sources were removed, except three potential cluster sources (22, 24, and 43).

¹ <https://heasarc.gsfc.nasa.gov/docs/software.html>

² <https://asc.harvard.edu/ciao/>

³ <http://heasarc.gsfc.nasa.gov/docs/xanadu/xspec/>

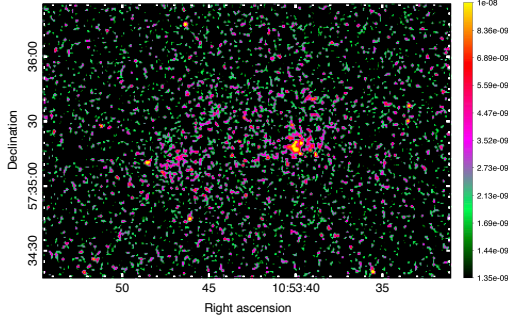


Figure 2. Broad band image with the reduced right ascension and declination ranges. Linear colorbar units are photons $\text{cm}^{-2} \text{s}^{-1}$.

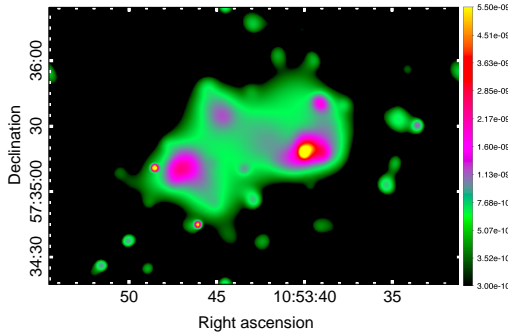


Figure 3. Adaptively-smoothed broad band image with undesired clusters removed. Uses scale: sqrt, zoom: fit, color: a, and scale parameters of $z_{\text{min}} = 3e-10$ and $z_{\text{max}} = 5.5e-09$. Linear colorbar units in $\text{cm}^2 \text{s}$.

The CIAO script `roi` was then used to create two region files made up of one excluding the background regions and one excluding the point source regions. These were verified using the CIAO script `DMMAKEREG` and visually inspecting these resulting region fit files within `ds9`. The CIAO routine `DMFILTH` was then used to fill in the source regions with average values determined by the background regions.

There was no significant difference between the versions including potential cluster sources (Figure 3) and the version with no sources. The NASA-IPAC Extragalactic Database (NED)⁴ was used to identify cluster sources 22, 24, and 43 as SSTS2 J105346.07+573445.1, SSTS2 J105348.49+573510.8, and WISEA J105340.14+573517.9, respectively. Source 43 is notable since it is the brightest cluster galaxy of the west subcluster and has a redshift of 1.135.

Two different methods were used to search for structures within the broad band no source images with normalized rates in the attempt of finding shocks. The first of these methods was via unsharp masking, which used the function `FGAUSS` with various levels of sharpness. `FARITH` was then used to subtract the widely smoothed images from the narrowly smoothed images. Nothing of importance was found when observing the unsharpened images in `DS9`. The second method was via the Gaussian gradient method, which

Table 2. Smoothed color image scaling parameters.

Band	Color	Scaling Type	Lower Limit (photons/ cm^2/s)	Upper Limit (photons/ cm^2/s)
Soft	Red	Square Root	1.3e-10	1.3e-09
Medium	Green	Logarithmic	9.9e-11	2.7e-09
Hard	Blue	Logarithmic	1e-10	2.1e-09

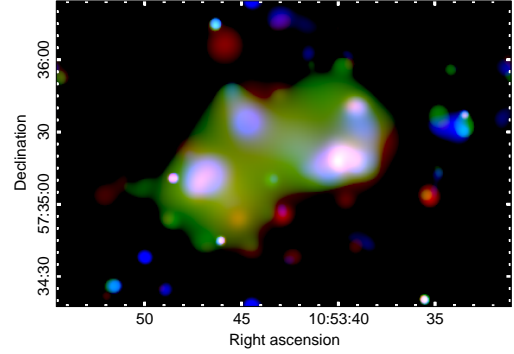


Figure 4. Smoothed soft, medium, and hard X-ray image using the specified scale parameters.

used the `GAUSSIAN_GRADIENT_MAGNITUDE` Python script. Similarly to the prior method, nothing much resulted from this.

The perl script `ASMOOTH_MATCHSCALE` was used to smooth each of the color images, which were separated into soft, medium, and hard. The final smoothed image fits files for soft, medium, and hard were opened in `ds9` using the `RGB` specifier along with specifiers designating soft (0.5-1.2 keV) as red, medium (1.2-2 keV) as green, and hard (2-7 keV) as blue. Various scaling options for the red, green, and blue X-rays were experimented with in order to minimize the surrounding noise, sharp edges, and white spots. The primary scaling types analyzed were square root and logarithmic. The final product had scale parameters specified in Table 2.

These scale parameters resulted in the image shown in Figure 4. A version without the medium X-rays was also produced using the same scaling parameters for soft and hard X-rays, which is shown in Figure 5. The differentiation between cool and hot areas was not as clear as hoped, and it is unlikely that there is a shock perpendicular to the line of sight. The trail seen in the upper left of the images is cooler rather than hotter, which signifies that it is likely cool gas from one of the centers of the clusters that has been pushed out by ram pressure during the merger.

Using the final broad band smoothed no source image, a spectra region file was created. This was accomplished using contour parameters within `DS9` and converting the contours to polygons. After this, all regions except the second-to-lowest contour polygon were deleted in order to end up with a contour encompassing the desired region, and this was saved as a region file.

3 CONCLUSION

The analysis comparing the `FAINT` mode observation from 2001 to the `VFAINT` mode observations from 2021-2022 proved useful in determining that the degradation of Chandra observations is acceptable over this time period. The merging of all nine observations proved successful and increased the total amount of usable data, which was used in further steps for producing images and attempt-

⁴ <http://ned.ipac.caltech.edu/>

□

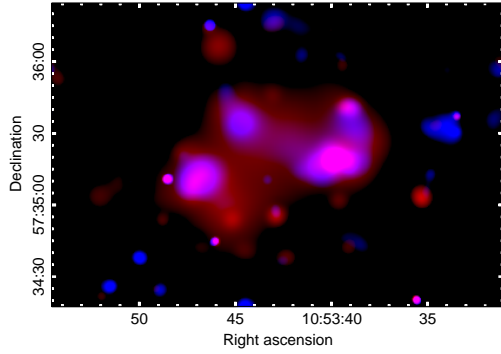


Figure 5. Smoothed soft and hard X-ray image using the specified scale parameters.

ing to determine shock locations. The cores of the clusters were softer, indicating that they're cooler, and the surrounding area was harder, indicating the opposite. The Chandra observations confirm the bimodal nature, and it appears to be undergoing a merger, but there is no clear evidence for a merger shock.

References: • Hashimoto, Y., et al., 2004, *A&A*, 417, 819 (Hash4) • Hashimoto, Y., et al., 2005, *A&A*, 439, 29 (Hash5) • Hasinger, G., et al., 1998a, *A&A*, 329, 482 • Markevitch, M., & Vikhlinin, A. 2007, *Phys. Rep.*, 443, 1 • Randall, S. W., Sarazin, C. L., & Ricker, P. M. 2002, *ApJ*, 577, 579 • Sarazin, C. L., Finoguenov, A., & Wik, D. R 2013, *AN*, 335, 346 • Wik, D., Sarazin, C., Ricker, P., & Randall, S. 2008, *ApJ*, 680, 17